Published source: J. Phys. D: Appl. Phys. 41 135208 (7 pages) (2008)

Electron transport in carbon tetrafluoride along a magnetically neutral plane between constant gradient antiparallel magnetic fields

Hirotake Sugawara and Yosuke Sakai

Division of Electronics for Informatics, Graduate School of Information Science and Technology, Hokkaido University, Sapporo 060-0814 Japan

Abstract. Electron motion in CF_4 at 0.67 Pa under crossed electric ($\boldsymbol{E}$) and magnetic ($\boldsymbol{B}$) fields was simulated by a Monte Carlo method to investigate fundamental properties of electron transport in neutral loop discharge plasmas for dry etching. As a simplified model of the electron path in the plasma, a magnetically neutral plane was assumed between linearly gradient antiparallel $\boldsymbol{B}$ fields, and a uniform $\boldsymbol{E}$ field was applied along the neutral plane perpendicularly to the $\boldsymbol{B}$ fields. The electron behaviour showed two contrasting modes depending on the direction of the $\boldsymbol{B}$ fields relative to the $\boldsymbol{E}$ field. In the field configuration which confines the electrons near the neutral plane, values of the mean electron energy, the drift velocity and the effective ionization frequency were close to those under the dc $\boldsymbol{E}$ field without $\boldsymbol{B}$ field. On the other hand, in the opposite $\boldsymbol{B}$ field configuration, the electrons hardly drifted along the $\boldsymbol{E}$ field, but instead, they showed a constant lateral diffusion driven by the $\boldsymbol{E} \times \boldsymbol{B}$ drift. A reverse-blocking effect of the gradient antiparallel $\boldsymbol{B}$ fields is reported.

PACS numbers: 52.20.-j Elementary processes in plasma, 52.20.Dq Particle orbits

Published source: J. Phys. D: Appl. Phys. 41 135208 (7 pages) (2008)

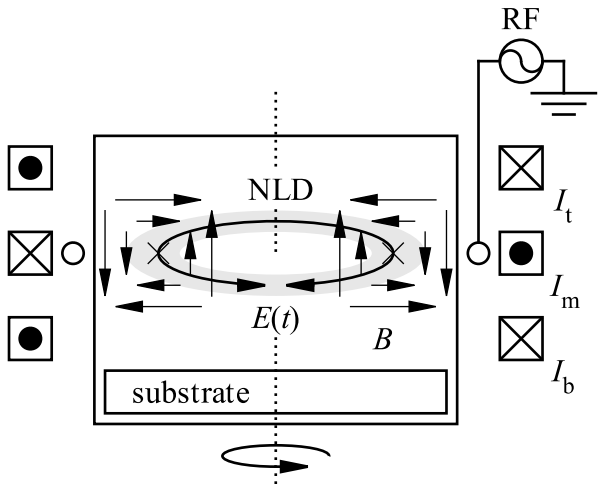

Figure 1. Schematic of cylindrical chamber and three-coil configuration for NLD plasma. The X points in the chamber represent the magnetically neutral positions.

1. Introduction

Demands for high-density plasmas driven at low pressures are increasing for finer and more economy dry processes of semiconductors. The neutral loop discharge (NLD) plasma is one of the most desirable plasma operation modes for the demands. For example, Tsuboi *et al* (1995, 1997) reported electron number densities n_e in the orders of 10^{16}–10^{17} m^{-3} in Ar at 0.067–0.13 Pa, and O'Connel *et al* (2007) reached n_e about 5×10^{17} m^{-3} in Ar at 1 Pa.

The NLD plasma is produced along a ring-shaped region of zero magnetic field, the so-called magnetic neutral loop (NL) (Tsuboi *et al* 1995 and Uchida 1998). The NL is formed usually by three coils placed coaxially around the cylindrical plasma chamber. As seen in figure 1, the direction of the middle coil current I_m is opposite to that of I_t and I_b for the top and bottom coils. The magnetic field induced by I_t and I_b is cancelled by that of I_m to form the NL, and resultingly the NL is surrounded by gradient magnetic fields.

Typical NLD plasmas are driven by a radio-frequency (RF, 13.56 MHz) electric power supplied inductively through an RF antenna, while some attempts to apply the

Published source: J. Phys. D: Appl. Phys. 41 135208 (7 pages) (2008)

NLD to RF capacitively coupled plasmas have also been made (Vural and Brinkmann 2007). Tsuboi and Ogata (2007) analysed an equivalent electrical circuit for an inductive NLD plasma. The plasma current was modelled to conduct along the NL, and the deposited plasma power was evaluated from the RF antenna voltage. Understanding of the electron behaviour around the NL is essential for development of advanced monitoring and control techniques of the NLD plasmas. However, microscopic electron behaviour around the NL analysed by Yoshida *et al* (1998) is complex and hard to interpret because of the complicated influence from the geometry of the electric and magnetic fields. Therefore, it is important to analyse elementary factors governing the electron transport along the NL.

In order to investigate fundamental features of the electron transport along the NL in low-pressure CF_4, we performed a Monte Carlo simulation in a simplified field configuration; we assumed a uniform dc electric field and linearly gradient antiparallel magnetic fields. In this paper, we present calculated results of electron transport parameters in CF_4 under the crossed electric and magnetic fields, and report the rectifying effect of the magnetic field on the electron drift.

2. Simulation model and conditions

2.1. Arrangement of electric and magnetic fields

The NL formed in an NLD plasma may be regarded as a line locally when its curvature radius is sufficiently large relative to a characteristic length of the electron flight such as the Larmor radius of the electron gyration. Thus, we let the y axis of real space (x, y, z) represent the NL, and we assume that the electric field $\boldsymbol{E}$ is applied in the y direction as

$$\boldsymbol{E} = (E_x, E_y, E_z) = (0, -E, 0) \quad (E = \text{constant} > 0). \tag{1}$$

The magnetic field $\boldsymbol{B}$ formed in practical NLD plasmas is quadrupole, as shown in figures 1 and 2(a). However, we reduce the $\boldsymbol{B}$ to have only B_z component as illustrated

Published source: J. Phys. D: Appl. Phys. 41 135208 (7 pages) (2008)

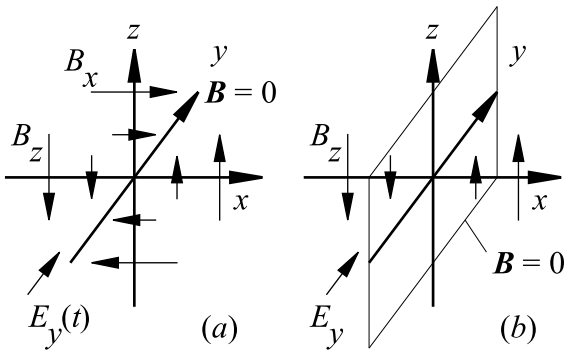

Figure 2. Electric and magnetic fields around magnetic neutral regions; (*a*) quadrupole $\boldsymbol{B}$ field around the y axis representing a part of the neutral loop in practical NLD plasmas and (*b*) simplified $\boldsymbol{B}$ field near the y-z plane representing the NC assumed for the present simulation.

in figure 2(*b*) in order to examine the effect of the B_z component separately from that of the B_x component. We let

$$\boldsymbol{B} = (B_x, B_y, B_z) = (0, 0, B_z(x)) \tag{2}$$

$$B_z(x) = \hat{B}_z x \quad (\hat{B}_z = \frac{\mathrm{d}}{\mathrm{d}x} B_z(x) = \text{constant}) \tag{3}$$

for simplicity. This configuration is equivalent to that analysed by Uchida (1998). Let us call the y-z plane, on which $\boldsymbol{B} = 0$, the 'neutral channel' (NC). The $\boldsymbol{B}$ fields on the both sides of the NC are antiparallel to each other. Such an arrangement of $\boldsymbol{B}$ can be realized between two equal parallel current slabs (Uchida 1998). In figure 3, two parallel current slabs with a width $2Z$ and a current density J per unit width along z are located at $x = \pm a$. $B_z(x)$ on the x axis is given analytically as

$$B_z(x) = \frac{\mu_0 J}{\pi} \arctan \frac{2Zx}{Z^2 + a^2 - x^2}, \tag{4}$$

where μ_0 is the permeability of free space. $B_z(x)$ can be approximated as a linear function as assumed in Uchida (1998):

$$B_z(x) \approx \frac{\mu_0 J}{\pi} \frac{2x}{Z} \quad \text{for } Z \gg x, a. \tag{5}$$

The linearity of a $\boldsymbol{B}$ component was also seen in a calculation result of the $\boldsymbol{B}$ field distribution around the NL by Gans *et al* (2007).

Published source: J. Phys. D: Appl. Phys. 41 135208 (7 pages) (2008)

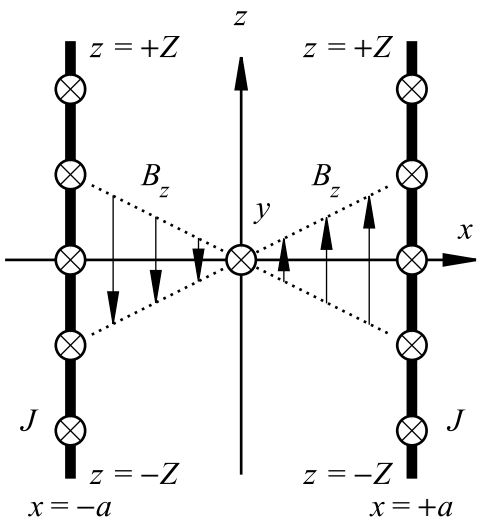

Figure 3. Magnetic field induced by two equal parallel current slabs with a current density J, a width $2Z$ and a separation $2a$.

Here, note that there are two possible arrangements for the $B_z(x)$ orientation relative to the direction of $\boldsymbol{E}$; whether the sign of $\hat{B}_z$ is positive or negative. When $\hat{B}_z > 0$, an electron flying toward the $+y$ direction turns inward to the NC under the action of the Lorentz force (figure 4(a)). On the other hand, when $\hat{B}_z < 0$, such an electron turns outward apart from the NC (figure 4(b)). Let us call these arrangements 'convergent' and 'divergent' configurations, respectively. These configurations can be also defined by the direction of the $\boldsymbol{E} \times \boldsymbol{B}$ drift. We will show the difference between the electron motions in these field configurations in the following section.

2.2. Monte Carlo simulation

CF_4, which is a representative etching gas, was chosen as the gas medium for the present simulation. The electron collision cross sections of CF_4 were taken from Kurihara *et al* (2000). The number density N of CF_4 molecules was set at 1.77×10^{14} cm^{-3} assuming a CF_4 pressure 0.67 Pa at 0°C. $\hat{B}_z$ was set at ± 0.5 mT cm^{-1}. We varied E in a range of 0.1–3.0 V cm^{-1}, which corresponds to the reduced electric field E/N of 57–1700 Td.

The initial electrons were released from the origin at $t = 0$ with energies subject to

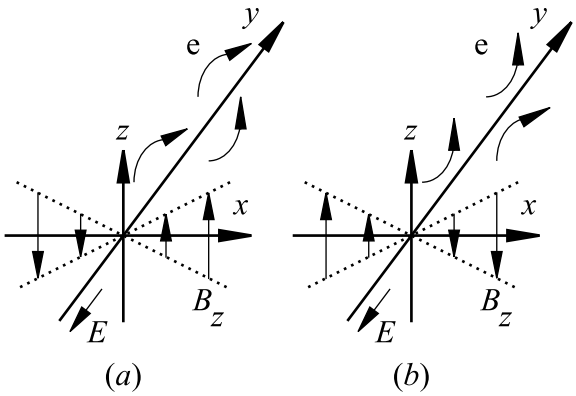

Figure 4. Magnetic field arrangements: (*a*) 'convergent' and (*b*) 'divergent' configurations.

a Maxwellian distribution of a mean energy of 1 eV. They were traced by a Monte Carlo code based on a Δt method, in which judgement of the occurrence of electron–molecule collisions and electron flight were repeated every unit simulation time $\Delta t = 3.7$ ps (1/20 000 of an RF period). Here, a timesaving scheme for the judgement of collisional events (Sugawara *et al* 2007) was adopted. The path of the electron flight under a spatially varying $\boldsymbol{B}$ field was calculated by applying the Runge–Kutta fourth order method to the following equations of motion:

$$\frac{\mathrm{d}}{\mathrm{d}t}\boldsymbol{r}_j = \boldsymbol{v}_j, \tag{6}$$

$$\frac{\mathrm{d}}{\mathrm{d}t}\boldsymbol{v}_j = -\frac{e}{m}\boldsymbol{E} - \frac{e}{m}\boldsymbol{v}_j \times \boldsymbol{B}, \tag{7}$$

where e and m are the electronic charge and mass, and $\boldsymbol{r}_j = (x_j, y_j, z_j)$ and $\boldsymbol{v}_j = (v_{x,j}, v_{y,j}, v_{z,j})$ are the position and velocity of the jth electron. The number of electrons sampled, n, was 10^6–10^7 in every condition.

The following electron swarm parameters were calculated from $\boldsymbol{r}_j$ and $\boldsymbol{v}_j$.

The mean electron energy $\bar{\varepsilon}$:

$$\bar{\varepsilon} = \frac{1}{n}\sum_{j=1}^{n}\varepsilon_j = \frac{1}{n}\sum_{j=1}^{n}\frac{m}{2}(v_{x,j}^2 + v_{y,j}^2 + v_{z,j}^2). \tag{8}$$

The effective ionization frequency ν_i:

$$\nu_\mathrm{i} = \frac{1}{n}\frac{\mathrm{d}}{\mathrm{d}t}n. \tag{9}$$

The centroid drift velocity W_r and the average velocity W_v:

$$W_\mathrm{r} = \frac{\mathrm{d}}{\mathrm{d}t} g_y = \frac{\mathrm{d}}{\mathrm{d}t} \left(\frac{1}{n} \sum_{j=1}^{n} y_j \right), \tag{10}$$

$$W_\mathrm{v} = \frac{1}{n} \sum_{j=1}^{n} v_{y,j}, \tag{11}$$

where g_y is the y component of the centroid position.

The diffusion coefficients $D_{E\times B}$, D_E and D_B defined in the directions of $\boldsymbol{E} \times \boldsymbol{B}$, $\boldsymbol{E}$ and $\boldsymbol{B}$, are respectively,

$$D_{E\times B} = \frac{1}{2} \frac{\mathrm{d}}{\mathrm{d}t} \left(\frac{1}{n} \sum_{j=1}^{n} x_j^2 \right), \tag{12}$$

$$D_E = \frac{1}{2} \frac{\mathrm{d}}{\mathrm{d}t} \left(\frac{1}{n} \sum_{j=1}^{n} (y_j - g_y)^2 \right), \tag{13}$$

$$D_B = \frac{1}{2} \frac{\mathrm{d}}{\mathrm{d}t} \left(\frac{1}{n} \sum_{j=1}^{n} z_j^2 \right). \tag{14}$$

Here, D_E is identical to the longitudinal diffusion coefficient D_L often defined in electron swarm analyses under dc $\boldsymbol{E}$ fields. Also, $D_{E\times B}$ and D_B correspond to the transverse diffusion coefficient D_T, but $D_{E\times B}$ and D_B may have different values under $\boldsymbol{E} \times \boldsymbol{B}$ fields. The electron diffusions in the x and z directions are symmetrical in $x = 0$ and $z = 0$, respectively.

3. Results and discussion

3.1. Electron flight loci

Two contrasting modes of the electron motion were observed. Figure 5 shows typical examples of electron loci for their flights of 1000 ns at $\hat{B}_z = \pm 0.5$ mT cm^{-1}.

In the convergent configuration, the electrons drift in the $+y$ direction meandering about the NC. The gradient antiparallel $\boldsymbol{B}$ fields confine the electrons near the NC. On the other hand, in the divergent configuration, the electrons hardly drift to the $+y$ direction for the gyration. Instead, the $\boldsymbol{E} \times \boldsymbol{B}$ drift occurs outward in the x direction. The gradient antiparallel $\boldsymbol{B}$ fields have a reverse-blocking effect on electron transport in the y direction.

Published source: J. Phys. D: Appl. Phys. 41 135208 (7 pages) (2008)

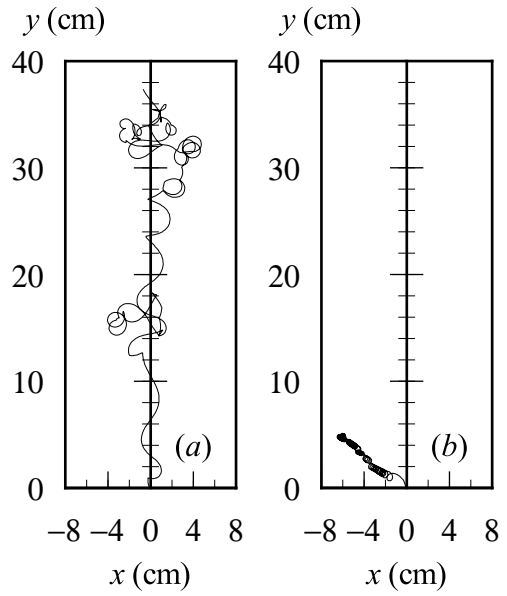

Figure 5. Loci of electron flights in CF_4 for 1000 ns in $\boldsymbol{E} \times \boldsymbol{B}$ fields of (*a*) convergent configuration ($\hat{B}_z = +0.5$ mT cm^{-1}) and (*b*) divergent configuration ($\hat{B}_z = -0.5$ mT cm^{-1}). $E = 1.0$ V cm^{-1}.

The confinement of electrons by the gradient antiparallel $\boldsymbol{B}$ fields in the convergent configuration is different from that by the magnetic mirror effect in the following point. The former is based on the $\boldsymbol{E} \times \boldsymbol{B}$ drift and its direction is perpendicular to $\boldsymbol{B}$, while the latter induces the electron reflection in the direction of $\boldsymbol{B}$.

3.2. Electron swarm parameters in the convergent configuration

Figures 6–9 show comparisons between electron swarm parameters in the $\boldsymbol{E} \times \boldsymbol{B}$ fields of the convergent configuration and those in dc $\boldsymbol{E}$ fields in the absence of the $\boldsymbol{B}$ field. The latter parameters were obtained from those in CF_4 at 133 Pa by conversions based on the similarity law of electron swarm parameters (ν_i/N, $\bar{\varepsilon}$, W_r, W_v, ND_L and ND_T are unique at a given E/N). Equilibrium values of $\bar{\varepsilon}$, ν_i, W_r and W_v in the convergent configuration were close to those under dc $\boldsymbol{E}$ fields of the same E/N. This was unchanged in supplementary simulations in which $\hat{B}_z$ was varied in a range 0.1–1.0 mT cm^{-1} at $E/N = 566$ Td. The diffusion coefficients D_E and D_B in figure 9

Published source: J. Phys. D: Appl. Phys. 41 135208 (7 pages) (2008)

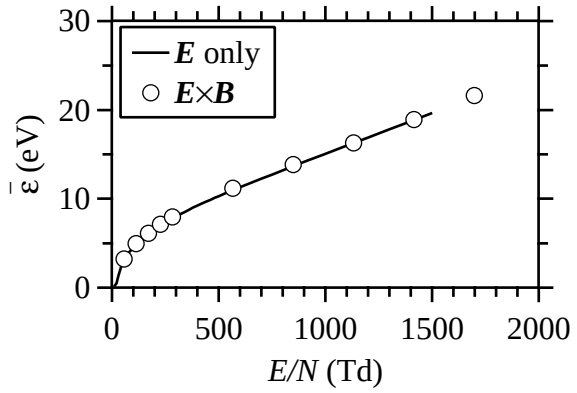

Figure 6. Mean electron energy $\bar{\varepsilon}$ in CF_4 under $\boldsymbol{E} \times \boldsymbol{B}$ fields of the convergent configuration at $\hat{B}_z = +0.5$ mT cm^{-1}.

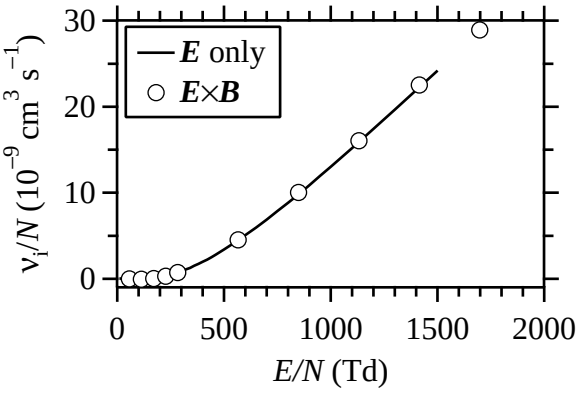

Figure 7. Reduced effective ionization frequency ν_i/N in CF_4 under $\boldsymbol{E} \times \boldsymbol{B}$ fields of the convergent configuration at $\hat{B}_z = +0.5$ mT cm^{-1}.

are also close to D_L and D_T, respectively, and only the values of $D_{E\times B}$ were negligibly small compared with D_E and D_B. The electrons moving away from the NC are reflected to the NC by the action of the inward $\boldsymbol{E} \times \boldsymbol{B}$ drift under the gradient $\boldsymbol{B}$ field, and the diffusion to the $\pm x$ directions is cancelled by this inward $\boldsymbol{E} \times \boldsymbol{B}$ drift. The average of v_x in each of the regions $x > 0$ and $x < 0$ is, respectively, zero (the total average of v_x is also zero), thus $D_{E\times B}$ is effectively zero.

In the situation of $D_{E\times B} = 0$, the spatial distribution of electrons in the x direction, $f(x)$, had a steady-state shape centred on the NC. The closeness of the transport

Published source: J. Phys. D: Appl. Phys. 41 135208 (7 pages) (2008)

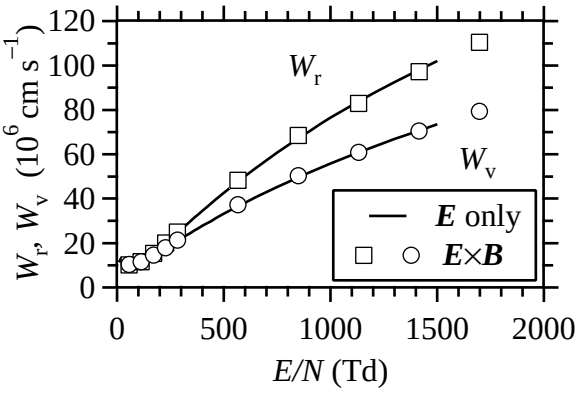

Figure 8. Electron drift velocities in CF_4 under $\boldsymbol{E} \times \boldsymbol{B}$ fields of the convergent configuration at $\hat{B}_z = +0.5$ mT cm^{-1}; the centroid drift velocity W_r and the average velocity W_v.

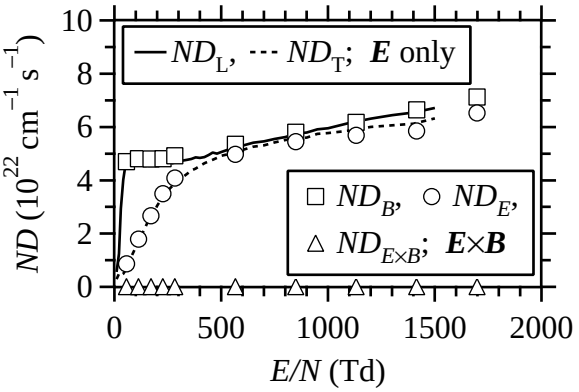

Figure 9. Electron diffusion coefficients in CF_4; $ND_{E\times B}$, ND_E and ND_B under the $\boldsymbol{E} \times \boldsymbol{B}$ fields of the convergent configuration at $\hat{B}_z = +0.5$ mT cm^{-1}; and ND_L and ND_T under dc $\boldsymbol{E}$ fields.

parameters in the convergent configuration to those in the $\boldsymbol{E}$ field only case is due to a feature that the electron transport along the $\boldsymbol{E}$ field is made mainly in a region of low $\boldsymbol{B}$ field. However, the transport parameters in the convergent configuration include more or less x-dependent factors reflecting the shape of $f(x)$ unlike those in hydrodynamic regime under uniform $\boldsymbol{E}$ and $\boldsymbol{B}$ fields. This would raise questions whether the values of the transport parameters presented here are substantial and whether the closeness is general. In addition to the preliminary result suggesting the insensitivity

Published source: J. Phys. D: Appl. Phys. 41 135208 (7 pages) (2008)

of the transport parameters to $\hat{B}_z$ reported above, further examination and theoretical study are necessary to answer these questions. Nonetheless, as long as the values of the transport parameters are unique to the given field conditions, they are meaningful quantities characterizing the electron conduction along the NC.

The $\boldsymbol{B}$ field deforms the electron energy distribution function as well, although there is no energy exchange between the electrons and the $\boldsymbol{B}$ field. Figure 10 shows the zeroth- and first-order terms, $F_0(\varepsilon)$ and $F_1(\varepsilon)$, of the Legendre polynomial expansion of the electron energy distribution function at $E/N = 113$ and 566 Td in the presence and absence of the $\boldsymbol{B}$ field. $F_0(\varepsilon)$ and $F_1(\varepsilon)$ represent the isotropic and directional components, respectively. They satisfies $\int_0^\infty F_0(\varepsilon)\mathrm{d}\varepsilon = 1$ (normalisation condition) and $W_\mathrm{v} = \frac{1}{3}\int_0^\infty v_1(\varepsilon/\varepsilon_1)^{1/2}F_1(\varepsilon)\mathrm{d}\varepsilon$, where $\varepsilon_1 = 1$ eV and v_1 is the electron speed associated with 1 eV.

A tendency common for $F_0(\varepsilon)$ at 113 and 566 Td is that the ratio of electrons with low energies near 0 eV increased in the $\boldsymbol{E} \times \boldsymbol{B}$ fields. $F_0(\varepsilon)$ and $F_1(\varepsilon)$ are less different at higher electron energies and at the higher E/N. This tendency can be explained by discussion in Dujko *et al* (2005) on a comparison between the cyclotron angular frequency ω and the collision frequency ν in CF_4. Dujko *et al* (2005) elucidated that the $\boldsymbol{B}$ field is less operative to the motion of high energy electrons of which $\nu \gg \omega$ (the collision-dominated regime) than to that of low energy electrons of $\nu \ll \omega$, for which it is difficult to gain energy from the $\boldsymbol{E}$ field for gyration (the $\boldsymbol{B}$ field-controlled regime). In the present field configuration, it is considered that electrons which lost their energy by inelastic collisions by chance in a region of a high $\boldsymbol{B}$ field underwent the difficulty in the regain of energy in the $\boldsymbol{B}$ field-controlled regime. A quantitative analysis for the spatial electron distribution with respect to the x direction and the x-dependent energy distribution will clarify details of the electron conduction along the NC. The reason why the electron swarm parameters do not change significantly even with the distortion of $F_0(\varepsilon)$ and $F_1(\varepsilon)$ would also be revealed by evaluating the effective $\boldsymbol{B}$ field operative to the swarm and the sensitivity of the parameters to changes of $F_0(\varepsilon)$ and $F_1(\varepsilon)$. These

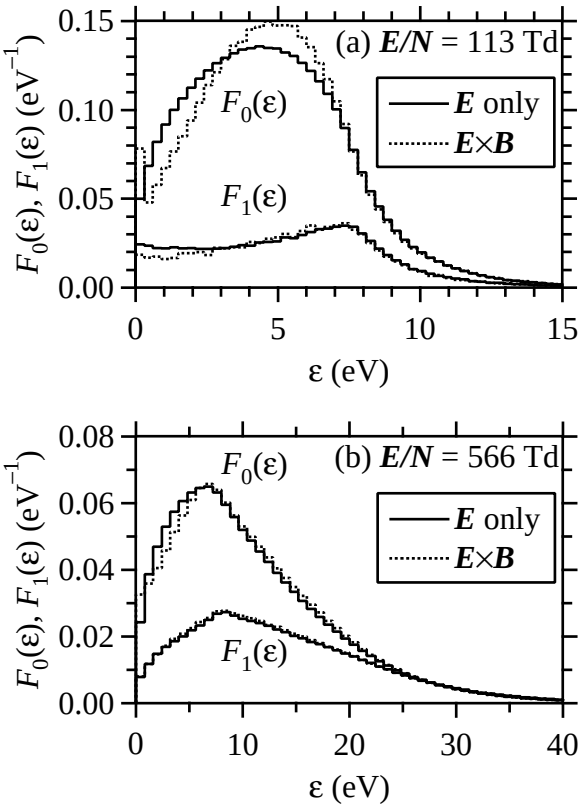

Figure 10. The isotropic and directional components $F_0(\varepsilon)$ and $F_1(\varepsilon)$ of the electron energy distribution function in CF_4 at (*a*) $E/N = 113$ and (*b*) 566 Td in the presence and absence of the $\boldsymbol{B}$ field.

issues will be interesting points in succeeding investigations.

3.3. Electron swarm parameters in the divergent configuration

In the divergent configuration ($\hat{B}_z < 0$), the electron drift toward the $+y$ direction was prevented and the electrons gain little energy. Electron swarm parameters $\bar{\varepsilon}$, ν_i, W_r, W_v, D_E and D_B decayed slowly in the electron energy loss process after the initial relaxation phase following the electron release, and their equilibrium values were not available in a trace of 7300 ns (= 100 RF cycles). Compared with the energy relaxation time in the dc $\boldsymbol{E}$ field at the present pressure, which is comparable to an RF cycle, the relaxation in the divergent configuration was slow by 1–2 orders of magnitude.

The only exception was $D_{E\times B}$. Figure 11 shows that $D_{E\times B}$ reached a constant

Published source: J. Phys. D: Appl. Phys. 41 135208 (7 pages) (2008)

value in a short relaxation time. We found that this constant value is represented as

$$D_{E\times B} = E/(-\hat{B}_z). \tag{15}$$

This relation can be derived analytically by assuming that the average electron velocity $\bar{v}_x(x)$ at position x is equal to the $\boldsymbol{E}\times\boldsymbol{B}$ drift velocity $E/(-\hat{B}_z x)$. This assumption is valid when the cyclotron period is much shorter than the electron mean free time. The present simulation condition satisfies this requirement. Then, the electron diffusion to the $\pm x$ directions proceeds as a result of the $\boldsymbol{E}\times\boldsymbol{B}$ drift, which is toward $x = +\infty$ in the region of $x > 0$ and toward $x = -\infty$ in $x < 0$. A derivation of $D_{E\times B}$ is presented in the appendix.

An interesting point of this result is that $D_{E\times B}$ in the divergent configuration is proportional to E, regardless of the gas species and N at sufficiently low pressures. This is different from the diffusion coefficients D_{L} and D_{T} under the dc $\boldsymbol{E}$ field only situation, under which D_{L} and D_{T} are inversely proportional to N at a given E/N (the similarity law). We consider that the independence of $D_{E\times B}$ from N is due to a fact that the electron diffusion with respect to the x direction occurs as a result of the $\boldsymbol{E}\times\boldsymbol{B}$ drift. Simulation results for the $\boldsymbol{E}\times\boldsymbol{B}$ drift velocity $W_{E\times B}$ in CF_4 (Sugawara *et al* 2000 and Dujko *et al* 2005) and an analytical expression for $W_{E\times B}$ (Li *et al* 2001), which can be rewritten as $W_{E\times B} = (E/B)/(\nu^2/\omega^2 + 1)$, indicate that $W_{E\times B}$ tends to E/B (a value independent of N) and is insensitive to N in a limit of low N in which $\nu \ll \omega$ ($\nu \propto N$).

4. Conclusions

Electron transport along a magnetically neutral plane (neutral channel, NC) between linearly gradient antiparallel $\boldsymbol{B}$ fields was simulated by a Monte Carlo method. Two different modes of the electron transport were observed depending on the direction of the $\boldsymbol{B}$ fields relative to the $\boldsymbol{E}$ field.

When the $\boldsymbol{E}\times\boldsymbol{B}$ direction is inward to the NC (the convergent configuration), the $\boldsymbol{B}$ field confines the electrons near the NC and the electron drift with energy gain occurs in a similar manner to that under dc $\boldsymbol{E}$ fields. Values of electron swarm parameters $\bar{\varepsilon}$,

Published source: J. Phys. D: Appl. Phys. 41 135208 (7 pages) (2008)

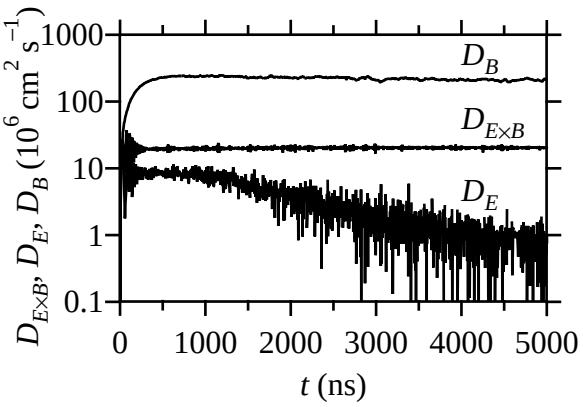

Figure 11. Temporal variation of the electron diffusion coefficients D_E, D_B and $D_{E\times B}$ in CF_4 at $E/N = 566$ Td under the $\boldsymbol{E}\times\boldsymbol{B}$ fields of the divergent configuration.

$\nu_{\rm i}$, $W_{\rm v}$ and $W_{\rm r}$ were close to those calculated at the same E/N values in dc $\boldsymbol{E}$ fields without $\boldsymbol{B}$ field. The diffusion coefficients D_E and D_B were also close to $D_{\rm L}$ and $D_{\rm T}$ in the dc $\boldsymbol{E}$ field, respectively, but $D_{E\times B}$ was negligibly small.

On the other hand, when the $\boldsymbol{E}\times\boldsymbol{B}$ direction is outward away from the NC (the divergent configuration), the $\boldsymbol{E}\times\boldsymbol{B}$ drift led the electrons into the regions of stronger $\boldsymbol{B}$ field. The electrons hardly drifted in the $-\boldsymbol{E}$ direction because of the large number of gyrations and they had little energy gain (reverse-blocking effect of the gradient antiparallel $\boldsymbol{B}$ fields on the electron transport along NC). Equilibrium values of the electron swarm parameters were not available, but it was found that only $D_{E\times B}$ has its equilibrium value $E/(-\hat{B}_z)$.

The field configuration in practical NLD plasmas is more complicated in two senses. The quadrupole $\boldsymbol{B}$ field involves both of the convergent and divergent configurations simultaneously; e.g. when the B_z component is in the convergent configuration, the B_x component is in the divergent one. In addition, the two configurations alternate every half an RF cycle with the polarity change of the $\boldsymbol{E}$ field. Since the relaxation time of the electron swarm parameters may be longer than the RF period at low pressures, the electron transport mode in practical NLD plasmas can be of transient. Consideration of these points is left for further investigation. The properties of electron transport

Published source: J. Phys. D: Appl. Phys. 41 135208 (7 pages) (2008)

under the effects of the gradient antiparallel $\boldsymbol{B}$ fields revealed in the present analysis are elementary but essential for better understanding of the electron behaviour in the NLD plasmas.

Acknowledgments

The author (HS) wishes to thank Drs S Ogata, H Tsuboi, Y Morikawa, K Kuwahara and K Tonari of ULVAC Inc. for valuable discussion on neutral loop discharge plasmas. This work was in part supported by Research Foundation for the Electrotechnology of Chubu.

Appendix A. Derivation of constant $D_{E\times B}$

We derive that the diffusion coefficient $D_{E\times B}$ defined in equation (12) becomes a constant in the field configuration of equations (1)–(3) ($\hat{B}_z < 0$) at a sufficiently low pressure.

We assume that the electron mean free time is much longer than the cyclotron period. At this time, the electron diffusion toward $x = \pm\infty$ is governed by the $\boldsymbol{E}\times\boldsymbol{B}$ drift. The diffusive velocity $\bar{v}_x(x)$ at a position x is equated to the $\boldsymbol{E}\times\boldsymbol{B}$ drift velocity $E/(-\hat{B}_z x)$.

$D_{E\times B}$ is calculated from the time derivative of the second-order moment $M_2(t)$ with respect to the position x normalized by the number of electrons $n(t)$ as

$$D_{E\times B} = \frac{1}{2}\frac{\mathrm{d}}{\mathrm{d}t}\frac{M_2(t)}{n(t)}. \tag{A.1}$$

With the electron position distribution $p(x,t)$, $n(t)$ and $M_2(t)$ are defined as follows:

$$n(t) = \int_{-\infty}^{\infty} p(x,t)\mathrm{d}x, \tag{A.2}$$

$$M_2(t) = \int_{-\infty}^{\infty} M_2(x,t)\mathrm{d}x = \int_{-\infty}^{\infty} x^2 p(x,t)\mathrm{d}x, \tag{A.3}$$

where $M_2(x,t)$ is a spatial distribution of the second-order moment.

On the other hand, the electron continuity equation with respect to the x direction is described using the electron flux $\bar{v}_x(x)p(x,t)$ and the source term $\nu_{\rm i}(x,t)p(x,t)$ as

$$\frac{\partial}{\partial t}p(x,t) = -\frac{\partial}{\partial x}[\bar{v}_x(x)p(x,t)] + \nu_{\rm i}(x,t)p(x,y). \tag{A.4}$$

$D_{E\times B}$ is derived as follows:

$$D_{E\times B} = \frac{1}{2}\frac{\frac{\rm d}{{\rm d}t}M_2(t)}{n(t)} - \frac{1}{2}\frac{\frac{\rm d}{{\rm d}t}n(t)}{n(t)}\frac{M_2(t)}{n(t)}, \tag{A.5}$$

$$= \frac{1}{2}\frac{1}{n(t)}\int_{-\infty}^{\infty} x^2\frac{\partial}{\partial t}p(x,t){\rm d}x - \frac{1}{2}\nu_{\rm i}(t)\frac{M_2(t)}{n(t)}, \tag{A.6}$$

$$= -\frac{1}{2}\frac{1}{n(t)}\int_{-\infty}^{\infty} x^2\frac{\partial}{\partial x}[\bar{v}_x(x)p(x,t)]{\rm d}x + \frac{1}{2}\frac{1}{n(t)}\int_{-\infty}^{\infty} x^2\nu_{\rm i}(x,t)p(x,t){\rm d}x - \frac{1}{2}\nu_{\rm i}(t)\frac{M_2(t)}{n(t)}, \tag{A.7}$$

$$= -\frac{1}{2}\frac{1}{n(t)}\left[x^2\bar{v}_x(x)p(x,t)\right]_{-\infty}^{\infty} + \frac{1}{n(t)}\int_{-\infty}^{\infty} x\bar{v}_x(x)p(x,t){\rm d}x + \frac{1}{2}\int_{-\infty}^{\infty}[\nu_{\rm i}(x,t) - \nu_{\rm i}(t)]\frac{M_2(x,t)}{n(t)}{\rm d}x. \tag{A.8}$$

The first term in equation (A.8) vanishes for a boundary condition $p(x,t) = 0$ at $x = \pm\infty$. The third term representing the non-uniformity of the generation and loss of the second-order moment is negligible when the ionization and electron attachment occur uniformly or rarely occur for low electron energy in the divergent configuration. Then, only the second term remains. By substituting the $\boldsymbol{E}\times\boldsymbol{B}$ drift velocity $E/(-\hat{B}_z x)$ to $\bar{v}_x(x)$ in the second term, $D_{E\times B}$ is obtained as

$$D_{E\times B} = \frac{1}{n(t)}\int_{-\infty}^{\infty}\frac{E}{-\hat{B}_z}p(x,t){\rm d}x = \frac{E}{-\hat{B}_z}. \tag{A.9}$$

References

Dujko S, Raspopović Z M and Petrović Z Lj 2005 *J. Phys. D: Appl. Phys.* **38** 2952–66

Gans T, Crintea D L, O'Connell D and Czarnetzki U 2007 *J. Phys. D: Appl. Phys.* **40** 4508–14

Kurihara M, Petrović Z Lj and Makabe T 2000 *J. Phys. D: Appl. Phys.* **33** 2146–53

Li B, White R D, Robson R E and Ness K F 2000 *Ann. Phys.* **292** 179–98

O'Connell D, Crintea D L, Gans T and Czarnetzki U 2007 *Plasma Sources Sci. Technol.* **16** 543–8

Sugawara H, Mori N, Sakai Y and Suda Y 2007 *J. Comp. Phys.* **223** 298–304

Sugawara H, Yahata T, Oda A and Sakai Y 2000 *J. Phys. D: Appl. Phys.* **33** 1191–6

Tsuboi H, Hayashi T and Uchida T 1997 *Japan. J. Appl. Phys.* **36** 6540–4

Published source: J. Phys. D: Appl. Phys. 41 135208 (7 pages) (2008)

Tsuboi H, Itoh M, Tanabe M, Hayashi T and Uchida T 1995 *Japan. J. Appl. Phys.* **34** 2476–81

Tsuboi H and Ogata S 2007 *Japan. J. Appl. Phys.* **46** 7475–7

Uchida T 1998 *J. Vac. Sci. Technol. A* **16** 1529–36

Vural M and Brinkmann R P 2007 *J. Phys. D: Appl. Phys.* **40** 510–9

Yoshida Z, Asakura H, Kakuno H, Morikawa J, Takenuma K, Takizawa S and Uchida T 1998 *Phys. Rev. Lett.* **81** 2458–61